Effects of electrode diameter and contact material on signal morphology of gastric bioelectrical slow wave recordings

Running Title: Effect of electrode diameter and material on slow waves

Authors & Affiliations:
Abhishek A. Kamat[1], Niranchan Paskaranandavadivel[1,2], Saeed Alighaleh[1], Leo K. Cheng[1,3], Timothy R. Angeli[1]

[1] Auckland Bioengineering Institute, University of Auckland, Auckland, New Zealand.
[2] Department of Surgery, University of Auckland, New Zealand
[3] Department of Surgery, Vanderbilt University, Nashville, TN, USA.

Correspondence
Dr Timothy R. Angeli
Auckland Bioengineering Institute
Private Bag 92019, Auckland, New Zealand
+64 9 923 1497; t.angeli@auckland.ac.nz

Final Published Citation:
Kamat AA, Paskaranandavadivel N, Alighaleh S, Cheng LK, Angeli TR. Effects of electrode diameter and contact material on signal morphology of gastric bioelectrical slow wave recordings. *Ann. Biomed. Eng.* 48(4):1407-1418, 2020.

Abstract:

Background: Gastric motility is governed in part by bioelectrical 'slow waves', and high-resolution electrical mapping has emerged as a clinical research tool with diagnostic potential. In this study, we aimed to determine the effects of electrode diameter and contact material on *in-vivo* extracellular slow wave recordings to inform gastric mapping device design. **Methods:** Custom flexible-printed-circuit electrode arrays were designed with four electrode diameters (0.3, 1.8, 3.3, 4.8 mm; 4x8 array) and fabricated in four contact materials (gold, silver, copper, silver-chloride). The electrode arrays were placed on the gastric serosa *in-vivo* in pigs and unipolar slow wave signals were simultaneously recorded from each electrode. Propagation, signal morphology, and noise were quantified to determine which electrodes produced signals with the highest signal-to-noise ratio (SNR) and gradient, which is a preferred metric for detection and analytical algorithms. **Results:** Electrodes of diameters 0.3 and 1.8 mm recorded significantly higher signal gradients than 3.3 and 4.8 mm ($p<0.05$). Silver-chloride electrodes recorded a significantly higher gradient than all other materials ($p<0.05$), with no significant differences between gold, silver, and copper electrodes. Electrodes of diameters 1.8 and 3.3 mm recorded significantly higher SNR than 0.3 mm ($p<0.05$). **Conclusions:** Electrodes with a diameter of 1.8 mm provided an optimal combination to maximise the signal gradient and SNR, and silver-chloride electrodes yielded the highest signal gradient. These results can now inform gastric mapping device design, particularly minimally-invasive devices where electrode size is critical.

Key terms: Electrophysiology; high-resolution mapping; electrode design; signal processing; gastrointestinal; slow wave; dysrhythmia;

Introduction

Gastric motility is initiated and coordinated in part by underlying rhythmic bioelectrical potentials, termed slow waves, that are generated and propagated by interstitial cells of Cajal.[24] Foundational knowledge on gastric slow waves was developed from studies that utilised low-resolution techniques, where a few electrodes were sparsely placed along the stomach or intestine.[3,23] The lack of spatial resolution allowed for analysis of temporal slow wave characteristics, like frequency, but prevented spatial propagation analysis. More recently, high-resolution mapping has been introduced, where dense arrays of many electrodes are placed on the stomach or intestines simultaneously to define slow wave activity in fine spatiotemporal resolution.[32]

High-resolution electrical mapping was first applied in the gastrointestinal (GI) tract by Lammers *et al.* in 1993 on the *in vivo* rabbit intestine, using a custom-built array of 240 teflon-coated silver wire electrodes (0.3 mm diameter, 15 x 16 array, 1 mm inter-electrode spacing) embedded in a rigid block of dental acrylic that was applied directly to the GI serosal surface.[25] Over the subsequent two decades, Lammers and his colleagues used a variety of custom-built electrode arrays to define spatiotemporal slow wave propagation characteristics in a range of *in vivo* and *in vitro* animal models.[26–28] In 2009, Du *et al.* developed sterilisable flexible-printed-circuit (FPC) electrode arrays (0.3 mm electrode diameter, gold contact),[18] enabling intra-operative application in human patients.[5,31] These electrode arrays have subsequently been applied to identify abnormalities of slow wave propagation, known as dysrhythmias, in post-surgical patients[11] and in patients with functional GI disorders, including gastroparesis[31] and chronic unexplained nausea and vomiting,[5] fuelling clinical interest in high-resolution mapping as a potential diagnostic tool.

Substantial GI research has been carried out using high-resolution mapping,[32] but little effort has been invested to define the effects of electrode design parameters on the quality of resultant extracellular GI signals. Optimization of the resultant signal amplitude and quality is particularly important for emerging minimally invasive endoscopic mapping techniques, where recordings from the gastric mucosal surface have substantially wider down-stroke width and lower amplitude (*i.e.*, lower signal-to-noise ratio, 'SNR') than serosal recordings.[6] High-resolution mapping arrays to date have primarily utilised electrodes of 0.3 mm diameter,[5,18,25] in silver or gold contact material.[18,25,33] Previous investigations on how electrode design parameters affect gastric slow wave signal morphology and quality have been restricted to a comparison of silver and gold contact material,[33] and the impact of electrode diameter has not been comprehensively evaluated.

In this study, we aimed to define the effects of electrode diameter and contact material on gastric slow wave signal morphology, to improve the resultant signal quality and inform future GI mapping device design.

Material and Methods

Electrode Array Design and Manufacture

A custom FPC template was designed in Altium Designer (v17; Altium, La Jolla, CA, USA). The FPC design is shown in Figure 1, and consisted of two sections: (i) the electrode contact-pad section (44 x 55 mm) composed of 32 electrodes of varying diameters, and (ii) the track section (360 x 16 mm) composed of tracks connecting the contact electrodes to their pins in the zero-insertion-force (ZIF) connector. Circular pads were used for electrode contacts, with electrode diameters of 0.3 mm, 1.8 mm, 3.3 mm and 4.8 mm. A diameter of 0.3 mm was selected as the minimum diameter based on the previous standard electrode diameter for slow wave recording.[18,25] The remaining diameters were increased linearly in uniform increments of 1.5 mm, as motivated by a previous cardiac electrophysiology modelling study,[40] and the total diameter range covered an order of magnitude increase in diameter (0.3 – 4.8 mm). The four different electrode diameters were spatially distributed across the electrode array as shown in Figure 1, mirrored across the mid-line of the central-axis to account for any regional slow wave variations within the mapped area.

An inter-electrode spacing of 7 mm was used for the FPC design. Inter-electrode spacing of 10 mm or less has been shown to be sufficient to accurately record slow wave propagation across a high-resolution GI mapping electrode array.[38] In this case, the largest electrode size of 4.8 mm needed to fit adjacently with four tracks in between, and the densest possible spacing was desired. The minimum inter-electrode spacing (MIS) was thereby calculated based on Equation 1:

$$\mathrm{MIS} = MD + 4 * TW + 3 * TTS + 2 * TES \qquad \text{(Eqn 1)}$$

where MD is the maximum electrode diameter of 4.8 mm in this case, TW is the track width (0.2 mm), TTS is the track-to-track spacing (0.3 mm), and TES is the track-to-electrode spacing (0.25 mm).

The FPC board material thickness was 0.13 mm, and a 3.5 mm spacing (*i.e.*, half of the inter-electrode distance) was placed between the outer electrodes of the array and the edge of the head section so that an equal inter-electrode distance would be maintained between adjacently tessellated arrays. The base material was Polyimide, and the inlaid tracks and connectors were copper (Type RA Cu 14.79 mL). The electrodes and connectors were surface plated with three different contact materials: silver, gold, and copper.

The FPCs were manufactured by PCBWay (Hangzhou, China), and the manufacture cost varied based on the surface contact material. The copper and gold finished electrodes cost US$190 per six FPCs and silver finished electrodes cost US$265 per 6 FPCs.

Initial recordings from the silver electrode arrays were found to contain a high level of noise. The silver electrodes were then ‘chloridized’ to create silver-chloride electrodes because chloridization has been shown to improve the signal quality and stability.[30] The electrode contact surface was cleaned with a 70% isopropyl alcohol wipe, and immersed in a sodium

hypochlorite solution (NaClO; *i.e.*, household grade bleach) for a period of 15 minutes, and then rinsed with tap water.[32]

Experimental Protocol

Ethical approval for porcine experiments was obtained from the University of Auckland Animal Ethics Committee. All recordings were performed *in vivo* in fasted, cross-bred, weaner pigs, which is an established model for GI slow wave mapping.[7,20] General anaesthesia was induced with Zoletil and maintained with isoflurane. Vital signs were continuously monitored and maintained within the normal range, including temperature, heart rate, and blood pressure. At the conclusion of each study, the pigs were euthanized by a bolus intravenous injection of sodium pentobarbital, while still under anaesthesia.

High-resolution mapping was performed with the custom designed electrode arrays using validated methods.[18,20,32] A laparotomy was performed to access the stomach, and the electrode arrays were placed on the corpus and/or antrum region of the gastric serosa. Warm, saline-soaked gauze was placed on top of the arrays to maintain contact with the serosa as well as abdominal moisture and temperature. All manipulations were performed with the minimal necessary gastric handling, and the wound edges were approximated with surgical clamps during the recording periods.

Each individual experiment was conducted using three tessellated electrode arrays (*i.e.*, 96 total electrodes), with each electrode array being plated in a different electrode contact material (*i.e.*, 32 electrodes of each material), as shown in Figure 1B. Recordings were performed in the corpus of the anterior and posterior surfaces of the stomach and the electrode array was rotated by 180˚ between each successive recording (Figure 2A), to further account for potential regional variations in slow wave activity within the mapped area.[20]

Signal Processing and Analysis

Unipolar electrical recordings were acquired from each electrode via an ActiveTwo system (BioSemi, Amsterdam, Netherlands) modified for passive recordings. Reference electrodes were placed on a shaved patch of the rear thigh, and custom software was used for the acquisition interface, written in LabView (National Instruments, Austin, TX, USA). Recordings were acquired at 512 Hz, then down sampled to 30 Hz for analysis.

Slow wave analyses were performed using the Gastrointestinal Electrical Mapping Suite (GEMS) v1.7 (FlexiMap, Auckland, New Zealand).[42] Recordings from the electrode arrays were filtered with a moving median filter (window size 20 s) to remove baseline drift and a Savitzky-Golay filter (polynomial order 9, window size 1.7 s) to remove high-frequency noise, previously validated for *in-vivo* extracellular gastric slow wave recordings.[34,35] Slow wave activation times (ATs) were identified and clustered into propagating cycles using validated automated methods, and propagation patterns were characterized by animation and isochronal AT maps.[42] Slow wave amplitude, downstroke width, frequency, and velocity were calculated using validated algorithms.[34,36,42] In particular, amplitude and downstroke width

were the primary features of signal morphology and were calculated by identifying the first peak and trough adjacent to the AT, using the zero crossing of the first derivative of the signal.[6,34]

Signals with high amplitude and narrow downstroke width are preferred because they are the key signatures of GI slow wave identification and analysis algorithms.[21,32,42] Slow wave amplitude and downstroke width are not necessarily inversely related, so the slow wave gradient was calculated to represent the combined effect of amplitude and downstroke width, as shown in Equation 2:

$$Gradient\ (mV/s) = \frac{Amplitude}{Downstroke\ Width} \qquad \text{(Eqn 2)}$$

The gradient thereby served as a combined metric of the signal quality, whereby a larger gradient signified the preferred signal morphology for slow wave detection and analysis (*i.e.*, high amplitude and narrow downstroke width).

To further investigate the effects of electrode dimeter and material on signal quality, SNR was calculated for each slow wave AT, as defined in Equation 3:

$$SNR = 20 * log_{10}\left(\frac{RMS_{signal}}{RMS_{noise}}\right) \qquad \text{(Eqn 3)}$$

where RMS_{signal} is the root mean square of the 1 s window centered around the slow wave AT (*i.e.*, 0.5 s before to 0.5 s after AT, which has been validated as an appropriate window to capture the downstroke width of the slow wave signal[6,7]), and RMS_{noise} is the root mean square of the 6 s window from 7 to 13 s after the slow wave AT (*i.e.*, 6 s window in the quiescent period between slow waves).[7,37]

Statistical Methods

Slow wave data were collated based on electrode material and/or diameter. Slow wave data were averaged across similar electrode materials and diameters within each recording, and then averaged across recordings, to enable comparisons between characteristics. Data were then represented as mean ± standard-error-of-the-means (SEM). Statistical comparisons of slow wave characteristics between the various electrode diameters and contact materials were performed by one-way ANOVA followed by post-hoc t-test.

Results

Data encompassed 20 recordings from four pigs (41 ± 0.3 kg; total recording duration 66.7 min; >8000 individual slow wave ATs). Data were acquired from all electrode materials and diameters. Example activation time, amplitude, downstroke width, and velocity maps are shown in Figure 2, and example slow wave signals are shown in Figure 3.

Effects of Electrode Diameter on Signal Morphology

The slow wave amplitudes and downstroke widths recorded by the electrode arrays are shown in Figure 4, represented as box plots for comparison across the range of electrode diameters that were tested (see also Supplementary Table S1). Slow wave signal amplitude from 0.3 mm versus 1.8 mm electrodes showed inconsistent trends across the different electrode contact materials (Figure 4A). A consistent trend of decreasing slow wave amplitude with increasing electrode diameter was observed from 1.8 mm to 4.8 mm electrode diameter, across all materials (Figure 4A). However, the only statistically significant difference was a lower amplitude from 4.8 mm copper electrodes, compared to all other diameters in that material.

Slow wave downstroke width consistently increased with each increase in diameter from 0.3 to 4.8 mm, across all electrode contact materials, with variable statistical significance as shown in Figure 4B.

The overall decrease in amplitude and increase in downstroke width with increasing electrode diameter suggests that the smaller electrode diameters of 0.3 and 1.8 mm produce the preferred slow wave signal morphology for optimum detection and analysis (i.e., a large, sharp downstroke).

Effects of Electrode Material on Signal Morphology

For comparison across the range of electrode materials, Figure 5 shows the slow wave amplitudes and downstroke widths recorded by the electrode arrays represented as box plots and grouped for each electrode diameter (see also Supplementary Table S1). Slow wave amplitude showed no consistent trends between electrode contact materials of copper, silver, and gold. Silver-chloride electrodes consistently resulted in higher median amplitude than all other materials, across all electrode diameters (Figure 5A), but the result was not statistically significant.

Slow wave downstroke width showed inconsistent trends between the electrode contact materials (Figure 5B), further highlighting the need for the combined slow wave gradient metric, presented below, to identify the electrode parameters that result in optimum slow wave morphology with large, sharp downstroke for detection and analysis.

Slow Wave Signal Gradient

The slow wave gradient represented the combined effects of amplitude and downstroke width to better elucidate how electrode diameter and material affect the desired slow wave

morphology with maximum gradient. The slow wave gradient versus electrode material is shown in Figure 6A, and gradient versus electrode diameter is shown in Figure 6B (see also Supplementary Table S2).

Silver-chloride electrodes produced the largest slow wave gradient, 21-28% higher than that recorded from the other materials, and there was no statistically significant difference between the gradient of signals recorded by copper, silver, or gold electrodes (Figure 6A; Supplementary Table S2). Electrodes with the smaller diameters of 0.3 and 1.8 mm recorded signals with a 17-47% higher gradient than the larger electrodes of 3.3 and 4.8 mm (Figure 6B; Supplementary Table S2). However, there was no statistically significant difference in the gradient recorded from electrodes of 0.3 versus 1.8 mm, or 3.3 versus 4.8 mm.

Signal-to-Noise Ratio (SNR)

The SNR represented the quality of the recording from each electrode, complimenting the slow wave amplitude, downstroke width, and gradient results by also including the impact of noise. The SNR versus electrode material is shown in Figure 7A, and SNR versus electrode diameter is shown in Figure 7B (see also Supplementary Table S3).

SNR was similar across all electrode materials, with only copper versus silver showing a statistically significant difference (copper electrodes had a 51% higher average SNR than silver; Figure 7A; Supplementary Table S3). The electrodes with a diameter of 1.8 and 3.3 mm recorded signals with a 26-59% higher SNR than the electrodes of 0.3 and 4.8 mm (Figure 7B; Supplementary Table S3).

Slow Wave Propagation

The mean slow wave frequency recorded across all electrodes was 3.6 ± 0.1 cycles per minute (cpm). There was no difference in the slow wave frequency recorded by the electrodes of any of the different diameters or materials ($p>0.05$ for all). The mean slow wave velocity across all electrode arrays was 6.6 ± 0.1 mm/s, and there was also no difference in the slow wave velocity calculated from electrodes of any of the different diameters or materials ($p>0.05$ for all).

Slow wave frequency and velocity are parameters of slow wave propagation rather than morphology. The consistency in frequency and velocity between the various electrodes was therefore expected, but is also consistent with previous reports of porcine gastric slow wave propagation,[6,20] suggesting validity of the slow wave data in this present study.

Discussion

In this study, custom electrode arrays were applied *in vivo* to the porcine stomach to elucidate the effects of electrode diameter and contact material on the resultant slow wave signal morphology. Each electrode array incorporated four different electrode diameters (0.3, 1.8, 3.3, 4.8 mm), and the arrays were fabricated in four surface contact materials (gold, silver, copper, and silver-chloride). Analysis algorithms to detect gastric slow wave ATs rely on a large amplitude and steep downstroke, so the preferred signal morphology is that with maximum amplitude and minimum downstroke width, *i.e.*, the maximum gradient, along with high SNR. Experimental results demonstrated that silver-chloride electrodes in the smaller diameters of 0.3 and 1.8 mm recorded signals with the highest gradient, and that all materials in the diameters of 1.8 and 3.3 mm recorded the highest SNR, therefore suggesting that these electrode characteristics are preferred for *in vivo* gastric recordings.

Electrode design considerations for GI recordings to date have typically been determined empirically, and have varied greatly from the early foundations by Alvarez *et al.*[3] in the 1920s to recent advancements in high-resolution mapping.[18,25,32] The two primary electrode design parameters are the electrode size and contact material. This study sought to advance the historic empirical foundation of these parameters with quantitative experimental analysis. Numerous conductive materials are available for the electrode material, which typically involve a trade-off between factors like biocompatibility, material properties, and conductivity.[30] Alvarez's initial GI electrical recordings were obtained using zinc-zinc sulfate moist thread electrodes.[3,4] Stainless steel and silver-silver-chloride were popular choices during the era of sparse electrode recordings,[15,23] but more recent high-resolution mapping technology has employed silver or gold electrode contacts.[18,25,33] Silver and gold are well established materials for bioelectrical applications, providing low impedance and stable electrode potential,[30] and have previously been shown to provide comparable signal quality when used for gastric serosal recordings.[33]

Our present study corroborates the fact that slow wave signal morphology is similar between silver and gold electrode contacts. However, it adds new findings that copper electrode contacts provide signal morphology consistent to that of silver and gold, and silver-chloride contacts provide higher-amplitude and steeper slow wave signals than silver, gold, or copper, with similar SNR from all materials. The fact that silver-chloride contacts provide improved signal morphology could be due to improved bridging and stable charge transfer at the electrolyte–electrode interface,[30] and investigating the relationship of electrical impedance versus frequency of GI slow wave recordings could be a valuable endeavour in future, as has historically been quantified in cardiac electrophysiology.[39] Importantly, our study now provides a definitive and quantitative definition of the improved morphology obtained from silver-chloride electrode contacts, and can now inform future device design. Our finding that copper electrode contacts offer similar signal morphology to silver and gold is also useful, demonstrating that electrode choices between those materials can be made based on other parameters, without sacrificing slow wave signal quality. For example, gold is more resistant

to corrosion during gastric pacing[2] or from sterilizing agents used in clinical applications.[32] Copper electrodes are typically less expensive and more efficient to manufacture than gold or silver, but are less biocompatible and have been shown to be toxic in implanted neural applications.[10,30]

The quantitative effects of electrode size on slow wave recordings had not previously been evaluated. An electrode diameter of 0.3 mm has been a common choice for both sparse electrode recordings,[14,23] and more recent high-resolution mapping.[18,25] Larger electrodes have also been used for serosal recordings, including 1 mm wide ring electrodes (2.2 mm ring diameter) for a recently-developed laparoscopic high-resolution mapping array.[12] Theoretically, the electrode size must strike a balance between having a large enough area to capture low-amplitude potentials versus being small enough to record the distinct steep activation potential (*i.e.*, downstroke) required for accurate event detection and subsequent spatiotemporal wavefront analysis.[21,42] Electrode size must also adhere to device design limitations, which is an area of growing interest in the GI field with the development of minimally-invasive laparoscopic[11,12] and endoscopic[6] mapping techniques that now require electrode arrays to be tightly packaged for delivery to the target region. Our present study now provides quantitative evaluation of the effects of electrode size on resultant slow wave signals. The smaller electrode diameters of 0.3 and 1.8 mm resulted in slow wave signals with higher amplitudes, narrower downstroke widths, and thereby higher gradients, than the larger electrodes of 3.3 and 4.8 mm; slow wave morphology differences between 0.3 versus 1.8 mm electrodes were inconsistent and/or not statistically significant. Electrodes of 1.8 and 3.3 mm resulted in higher SNR than those of 0.3 and 4.8 mm; SNR differences between 1.8 versus 3.3 mm electrodes were inconsistent and/or not statistically significant. These results thereby suggest that smaller diameter electrodes down to 0.3 mm are equally or more effective at recording gastric slow waves than larger electrodes, although slightly larger electrodes around 1.8 mm may improve SNR over the smaller diameter electrodes. These results demonstrate that the quality of slow wave morphology is not sacrificed when using smaller electrode diameters for minimally invasive recording devices, but gains in SNR may be obtained from slight increase in electrode size.

This study provides a methodological platform for assessing the effects of electrode design parameters on resultant signal morphology and quality, which could now be expanded and applied to other research areas in future studies. Our study was specifically focused on gastric slow waves recorded from the serosal surface, but the results may likely also apply to other regions of the gut, including the small intestine[1,8,9] and mucosal surfaces.[6] The methodology developed in this study may be useful to inform similar studies on electrode design for other fields of smooth muscle electrophysiology, for example in the bladder[22] and uterus.[29] There is also substantial scope for computational modelling in this area, as has been usefully applied to gastric and small intestine electrophysiology in recent years,[16,17,19] and could now be utilized to further investigate the effects of electrode design parameters. For example, the mechanism by which the smaller electrodes in this study recorded higher amplitude signals

than the larger electrode sizes is not fully defined, but could be due to the smaller recording area of the electrode array enabling more of the electrode to be in contact with the activated tissue of a propagating slow wave. These concepts could be modelled in future studies to better elucidate mechanisms of action of resultant slow wave signals, similar to existing models of the slow wave morphology resulting from flush extracellular contact electrodes versus extracellular suction electrodes.[7]

Four discrete electrode diameters were tested in our present study, which demonstrated a range of effective electrode diameters but was not able to identify a discrete optimal electrode size; this would be a useful aim for future investigations. Although the results encompassed 20 recordings and more than 8000 individual slow wave ATs, these data were collected from a relatively limited sample size of four porcine subjects. Additionally, the electrode arrays used in our study were composed of flush electrode contacts. It would be valuable to explore the impact of protruding electrodes in the future, which have previously been used for sparse *in vivo* recordings,[15] and are recommended for high-resolution *in vitro* recordings to maintain perfusion of the mapped tissue region in the tissue-bath.[25] Additional electrode materials could also be trialled in future. For example, platinum-iridium offers excellent stability, biocompatibility, and conductivity, but is expensive and can be difficult to fabricate into high-resolution arrays. Polymer based electrodes like poly-(3,4-ethylenedioxythiophene) (PEDOT) and indium tin oxide (ITO) have demonstrated promising results in other fields, including cardiac electrophysiology, and feature stretchable transparent characteristics that may be useful for future GI applications as well.[13,41]

In conclusion, this study improves our understanding of the quantitative effects of electrode design parameters on gastric slow wave morphology. The results can now be used to inform future device design for clinical gastric mapping tools that aim to detect abnormal electrical activation patterns in patients with gastric disorders.

Acknowledgements: The authors thank Dr Peng Du and Linley Nisbet for their expert assistance with this study.

Funding: This project and/or authors were supported by research grants from the Kelliher Charitable Trust, the Auckland Medical Research Foundation, the New Zealand Health Research Council (HRC), the MedTech Centre of Research Excellence New Zealand, and the Riddet Institute Centre of Research Excellence New Zealand. TRA was supported by the Edith C. Coan Postdoctoral Fellowship from the Auckland Medical Research Foundation and Rutherford Discovery Fellowship from the Royal Society of New Zealand.

Conflict of Interest: LKC, NP, and TRA hold intellectual property in the field of gastrointestinal electrophysiology and are shareholders in FlexiMap Ltd. AAK and SA declare no conflicts of interest. No commercial financial support was provided for this study.

References

1. Abraham, A. C., L. K. Cheng, T. R. Angeli, S. Alighaleh, and N. Paskaranandavadivel. Dynamic slow-wave interactions in the rabbit small intestine defined using high-resolution mapping. *Neurogastroenterol. Motil.* 31:e13670, 2019.
2. Alighaleh, S., L. K. Cheng, T. R. Angeli, M. Amiri, S. Sathar, G. O'Grady, and N. Paskaranandavadivel. A novel gastric pacing device to modulate slow waves and assessment by high-resolution mapping. *IEEE Trans. Biomed. Eng.* [Epub ahead of print], 2019.doi:10.1109/TBME.2019.2896624
3. Alvarez, W. C. The electrogastrogram and what it shows. *J. Am. Med. Assoc.* 78:1116–1119, 1922.
4. Alvarez, W. C., and L. J. Mahoney. Action currents in stomach and intestine. *Am. J. Physiol.* 58:476–493, 1922.
5. Angeli, T. R., L. K. Cheng, P. Du, T. H.-H. Wang, C. E. Bernard, M.-G. Vannucchi, M. S. Faussone-Pellegrini, C. Lahr, R. Vather, J. A. Windsor, G. Farrugia, T. L. Abell, and G. O'Grady. Loss of interstitial cells of Cajal and patterns of gastric dysrhythmia in patients with chronic unexplained nausea and vomiting. *Gastroenterology* 149:56-66.e5, 2015.
6. Angeli, T. R., P. Du, N. Paskaranandavadivel, A. Hall, S. J. Asirvatham, G. Farrugia, J. A. Windsor, L. K. Cheng, and G. O'Grady. High-resolution electrical mapping of porcine gastric slow-wave propagation from the mucosal surface. *Neurogastroenterol. Motil.* 29:e13010, 2017.
7. Angeli, T. R., P. Du, N. Paskaranandavadivel, P. W. M. Janssen, A. Beyder, R. G. Lentle, I. P. Bissett, L. K. Cheng, and G. O'Grady. The bioelectrical basis and validity of gastrointestinal extracellular slow wave recordings. *J. Physiol.* 591:4567–4579, 2013.
8. Angeli, T. R., G. O'Grady, N. Paskaranandavadivel, J. C. Erickson, P. Du, A. J. Pullan, I. P. Bissett, and L. K. Cheng. Experimental and automated analysis techniques for high-resolution electrical mapping of small intestine slow wave activity. *J. Neurogastroenterol. Motil.* 19:179–191, 2013.
9. Angeli, T. R., G. O'Grady, R. Vather, I. P. Bissett, and L. K. Cheng. Intra-operative high-resolution mapping of slow wave propagation in the human jejunum: Feasibility and initial results. *Neurogastroenterol. Motil.* e13310, 2018.doi:10.1111/nmo.13310
10. Babb, T. L., and W. Kupfer. Phagocytic and metabolic reactions to chronically implanted metal brain electrodes. *Exp. Neurol.* 86:171–182, 1984.
11. Berry, R., L. K. Cheng, P. Du, N. Paskaranandavadivel, T. R. Angeli, T. Mayne, G. Beban, and G. O'Grady. Patterns of abnormal gastric pacemaking after sleeve gastrectomy defined by laparoscopic high-resolution electrical mapping. *Obes. Surg.* 27:1929–1937, 2017.
12. Berry, R., N. Paskaranandavadivel, P. Du, M. L. Trew, G. O'Grady, J. A. Windsor, and L. K. Cheng. A novel retractable laparoscopic device for mapping gastrointestinal slow wave propagation patterns. *Surg. Endosc.* 31:477–486, 2016.
13. Bihar, E., T. Roberts, E. Ismailova, M. Saadaoui, M. Isik, A. Sanchez-Sanchez, D. Mecerreyes, T. Hervé, J. B. De Graaf, and G. G. Malliaras. Fully printed electrodes on stretchable textiles for long-term electrophysiology. *Adv. Mater. Tech.* 2:2–6, 2017.
14. Bozler, E. The action potentials of the stomach. *Am. J. Physiol.* 144:693–700, 1945.
15. Code, C. F., and J. A. Marlett. The interdigestive myo-electric complex of the stomach

and small bowel of dogs. *J. Physiol.* 246:289–309, 1975.

16. Du, P., S. Calder, T. R. Angeli, S. Sathar, N. Paskaranandavadivel, G. O'Grady, and L. K. Cheng. Progress in mathematical modeling of gastrointestinal slow wave abnormalities. *Front. Physiol.* 8:1136, 2018.
17. Du, P., A. Hameed, T. R. Angeli, C. Lahr, T. L. Abell, L. K. Cheng, and G. O'Grady. The impact of surgical excisions on human gastric slow wave conduction, defined by high-resolution electrical mapping and in silico modeling. *Neurogastroenterol. Motil.* 27:1409–1422, 2015.
18. Du, P., G. O'Grady, J. U. Egbuji, W. J. E. P. Lammers, D. Budgett, P. Nielsen, J. A. Windsor, A. J. Pullan, and L. K. Cheng. High-resolution mapping of in vivo gastrointestinal slow wave activity using flexible printed circuit board electrodes: methodology and validation. *Ann. Biomed. Eng.* 37:839–846, 2009.
19. Du, P., N. Paskaranandavadivel, T. R. Angeli, L. K. Cheng, and G. O'Grady. The virtual intestine: in silico modeling of small intestinal electrophysiology and motility and the applications. *WIREs Syst. Biol. Med.* 8:69–85, 2016.
20. Egbuji, J. U., G. O'Grady, P. Du, L. K. Cheng, W. J. E. P. Lammers, J. A. Windsor, and A. J. Pullan. Origin, propagation and regional characteristics of porcine gastric slow wave activity determined by high-resolution mapping. *Neurogastroenterol. Motil.* 22:e292-300, 2010.
21. Erickson, J. C., G. O'Grady, P. Du, C. Obioha, W. Qiao, W. O. Richards, L. A. Bradshaw, A. J. Pullan, and L. K. Cheng. Falling-edge, variable threshold (FEVT) method for the automated detection of gastric slow wave events in high-resolution serosal electrode recordings. *Ann. Biomed. Eng.* 38:1511–1529, 2010.
22. Hammad, F. T., B. Stephen, L. Lubbad, J. F. B. Morrison, and W. J. Lammers. Macroscopic electrical propagation in the guinea pig urinary bladder. *Am. J. Physiol. Ren. Physiol.* 307:F172–F182, 2014.
23. Hinder, R. A., and K. A. Kelly. Human gastric pacesetter potential. Site of origin, spread, and response to gastric transection and proximal gastric vagotomy. *Am. J. Surg.* 133:29–33, 1977.
24. Huizinga, J. D., and W. J. E. P. Lammers. Gut peristalsis is governed by a multitude of cooperating mechanisms. *Am. J. Physiol. Gastrointest. Liver Physiol.* 296:G1-8, 2009.
25. Lammers, W. J. E. P., A. Al-Kais, S. Singh, K. Arafat, and T. Y. El-Sharkawy. Multielectrode mapping of slow-wave activity in the isolated rabbit duodenum. *J. Appl. Phys.* 74:1454–1461, 1993.
26. Lammers, W. J. E. P., L. Ver Donck, J. A. J. Schuurkes, and B. Stephen. Peripheral pacemakers and patterns of slow wave propagation in the canine small intestine in vivo. *Can. J. Physiol. Pharmacol.* 83:1031–1043, 2005.
27. Lammers, W. J. E. P., L. Ver Donck, B. Stephen, D. Smets, and J. A. J. Schuurkes. Focal activities and re-entrant propagations as mechanisms of gastric tachyarrhythmias. *Gastroenterology* 135:1601–1611, 2008.
28. Lammers, W. J. E. P., L. Ver Donck, B. Stephen, D. Smets, and J. A. J. Schuurkes. Origin and propagation of the slow wave in the canine stomach: the outlines of a gastric conduction system. *Am. J. Physiol. Gastrointest. Liver Physiol.* 296:G1200-1210, 2009.
29. Lammers, W. J. E. P., B. Stephen, M. A. Al-Sultan, S. B. Subramanya, and A. M. Blanks. The location of pacemakers in the uteri of pregnant guinea pigs and rats. *Am. J.*

Physiol. Regul. Integr. Comp. Physiol. 309:R1439–R1446, 2015.

30. McAdams, E. Bioelectrodes. In: Encyclopedia of Medical Devices and Instrumentation, edited by J. G. Webster. New York: Wiley, 2006, pp. 120–166.
31. O'Grady, G., T. R. Angeli, P. Du, C. Lahr, W. J. E. P. Lammers, J. A. Windsor, T. L. Abell, G. Farrugia, A. J. Pullan, and L. K. Cheng. Abnormal initiation and conduction of slow-wave activity in gastroparesis, defined by high-resolution electrical mapping. *Gastroenterology* 143:589-598.e1–3, 2012.
32. O'Grady, G., T. R. Angeli, N. Paskaranandavadivel, J. C. Erickson, C. Wells, A. A. Gharibans, L. K. Cheng, and P. Du. Methods for high-resolution electrical mapping in the gastrointestinal tract. *IEEE Rev. Biomed. Eng.* 12:287–302, 2019.
33. O'Grady, G., N. Paskaranandavadivel, T. R. Angeli, P. Du, J. A. Windsor, L. K. Cheng, and A. J. Pullan. A comparison of gold versus silver electrode contacts for high-resolution gastric electrical mapping using flexible printed circuit board arrays. *Physiol. Meas.* 32:N13-22, 2011.
34. Paskaranandavadivel, N., L. K. Cheng, P. Du, G. O'Grady, and A. J. Pullan. Improved signal processing techniques for the analysis of high resolution serosal slow wave activity in the stomach. *Conf. Proc. IEEE. Eng. Med. Biol. Soc.* 1:1737–1740, 2011.
35. Paskaranandavadivel, N., G. O'Grady, P. Du, and L. K. Cheng. Comparison of filtering methods for extracellular gastric slow wave recordings. *Neurogastroenterol. Motil.* 25:79–83, 2013.
36. Paskaranandavadivel, N., G. O'Grady, P. Du, A. J. Pullan, and L. K. Cheng. An improved method for the estimation and visualization of velocity fields from gastric high-resolution electrical mapping. *IEEE. Trans. Biomed. Eng.* 59:882–889, 2012.
37. Paskaranandavadivel, N., X. Pan, P. Du, G. O'Grady, and L. K. Cheng. Detection of the recovery phase of in vivo gastric slow wave recordings. *Conf. Proc. IEEE. Eng. Med. Biol. Soc.* 1:6094–6097, 2015.
38. Putney, J., G. O'Grady, T. R. Angeli, N. Paskaranandavadivel, L. K. Cheng, J. C. Erickson, and P. Du. Determining the efficient inter-electrode distance for high-resolution mapping using a mathematical model of human gastric dysrhythmias. *Conf. Proc. IEEE. Eng. Med. Biol. Soc.* 2015:1448–1451, 2015.
39. Spach, M. S., R. C. Barr, J. W. Havstad, and E. C. Long. Skin-electrode impedance and its effect on recording cardiac potentials. *Circulation* 34:649–656, 1966.
40. Stinnett-Donnelly, J. M., N. Thompson, N. Habel, V. Petrov-Kondratov, D. D. Correa De Sa, J. H. T. Bates, and P. S. Spector. Effects of electrode size and spacing on the resolution of intracardiac electrograms. *Coron. Artery Dis.* 23:126–132, 2012.
41. Vosgueritchian, M., D. J. Lipomi, and Z. Bao. Highly conductive and transparent PEDOT:PSS films with a fluorosurfactant for stretchable and flexible transparent electrodes. *Adv. Funct. Mater.* 22:421–428, 2012.
42. Yassi, R., G. O'Grady, N. Paskaranandavadivel, P. Du, T. R. Angeli, A. J. Pullan, L. K. Cheng, and J. C. Erickson. The gastrointestinal electrical mapping suite (GEMS): software for analyzing and visualizing high-resolution (multi-electrode) recordings in spatiotemporal detail. *BMC Gastroenterol.* 12:60, 2012.

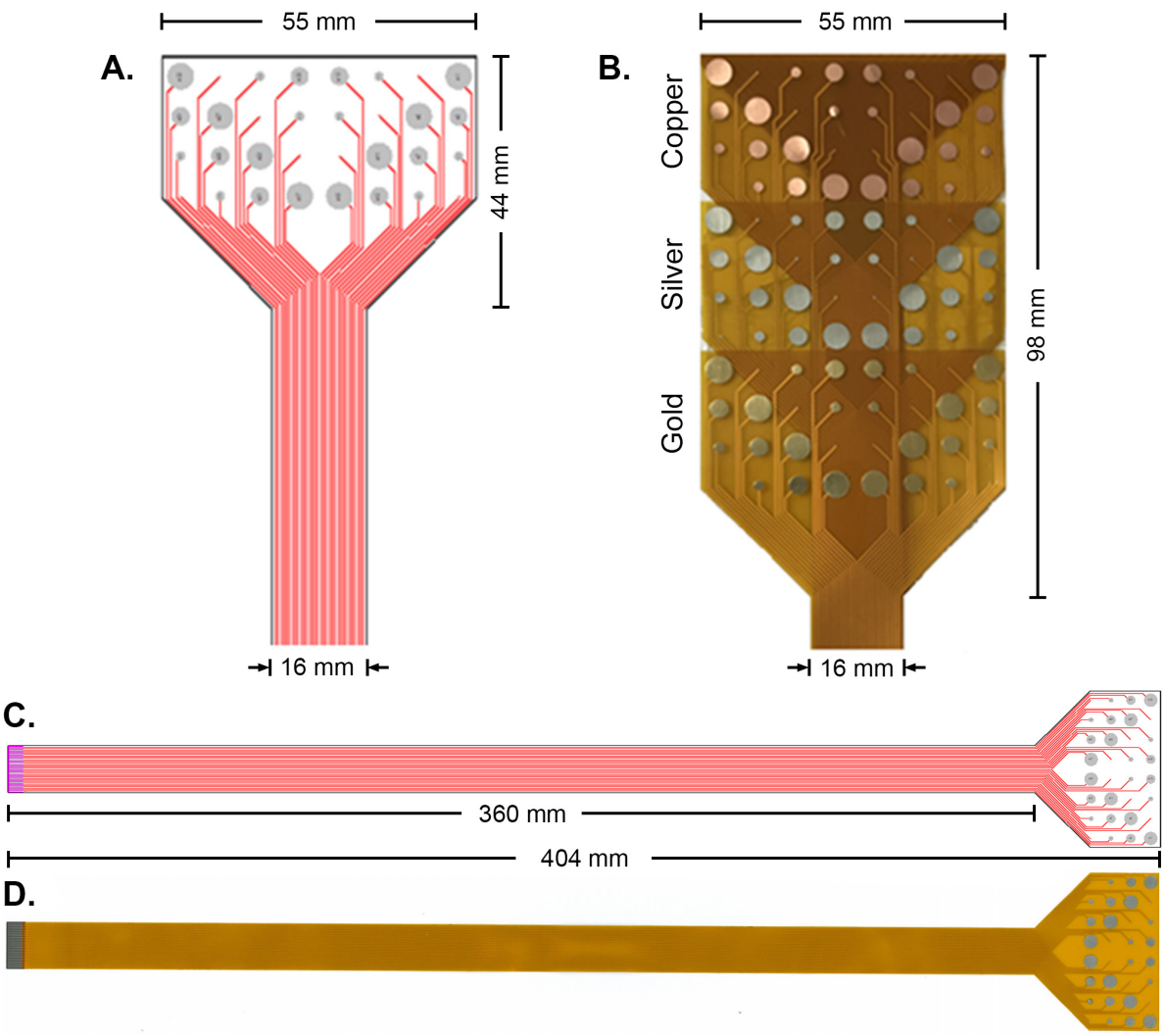

Figure 1: A. Design of FPC electrode array with four different diameters (0.3, 1.8, 3.3, 4.8 mm). **B.** Tessellated electrode arrays fabricated in three contact materials: copper, silver, and gold. **C.** Finalised electrode array design. **D.** Fabricated electrode array for in-vivo experiments.

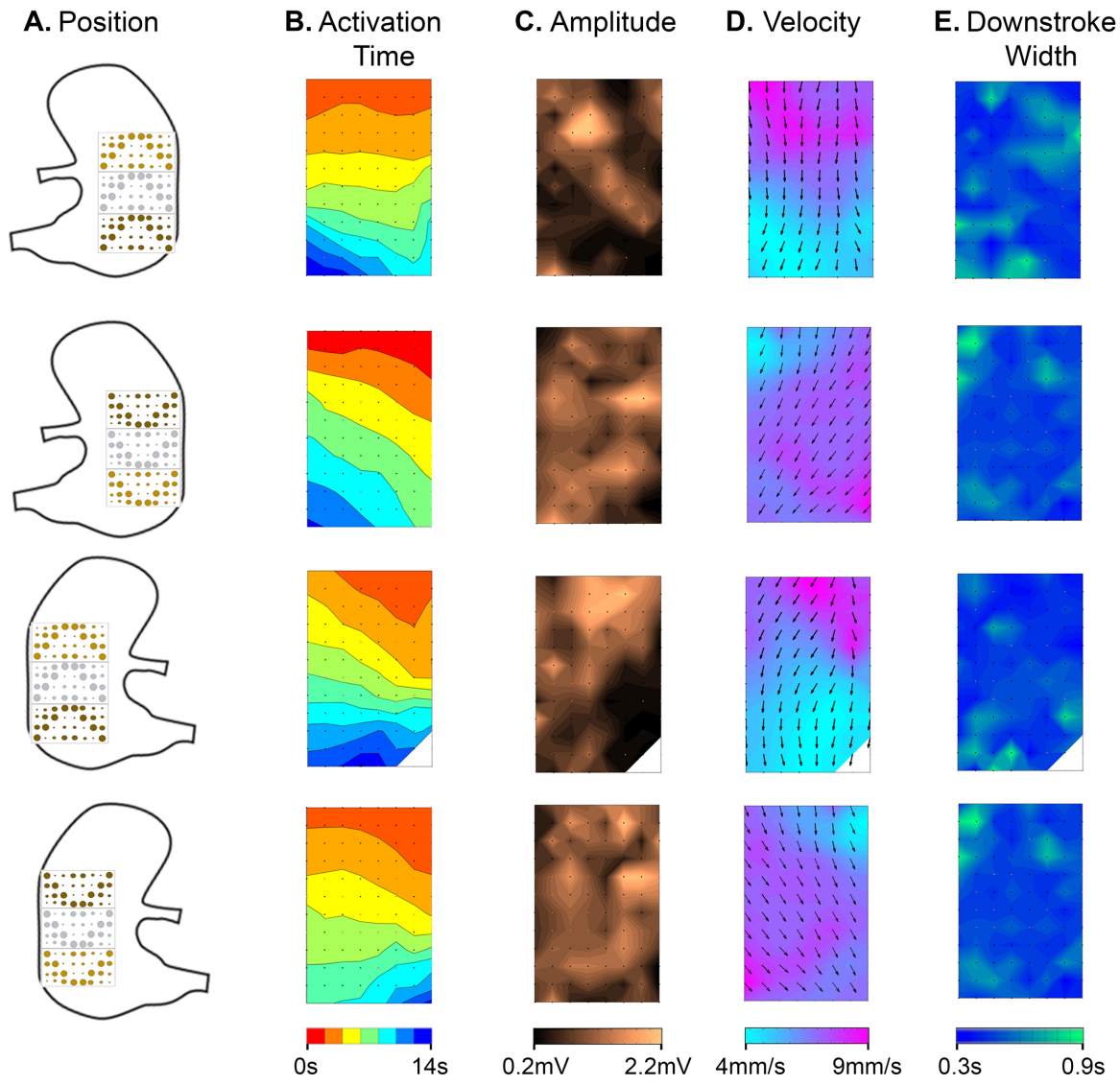

Figure 2: Experimental mapping results from electrode arrays. **A.** Positioning of the mapping arrays on the anterior (top two panels) and posterior (bottom two panels) stomach surfaces, with 180˚ rotations to account for regional differences. Mapping results include: **B.** AT maps, where each dot represents an electrode and each color band shows the area of propagation per 2 s from red (early) to blue (late); **C.** Amplitude maps, where the amplitude at each electrode is shown as a color gradient; **D.** Velocity maps, where propagation direction is shown with an arrow and speed is shown as a color gradient; **E.** Downstroke width maps, where the downstroke width at each electrode is shown as a color gradient.

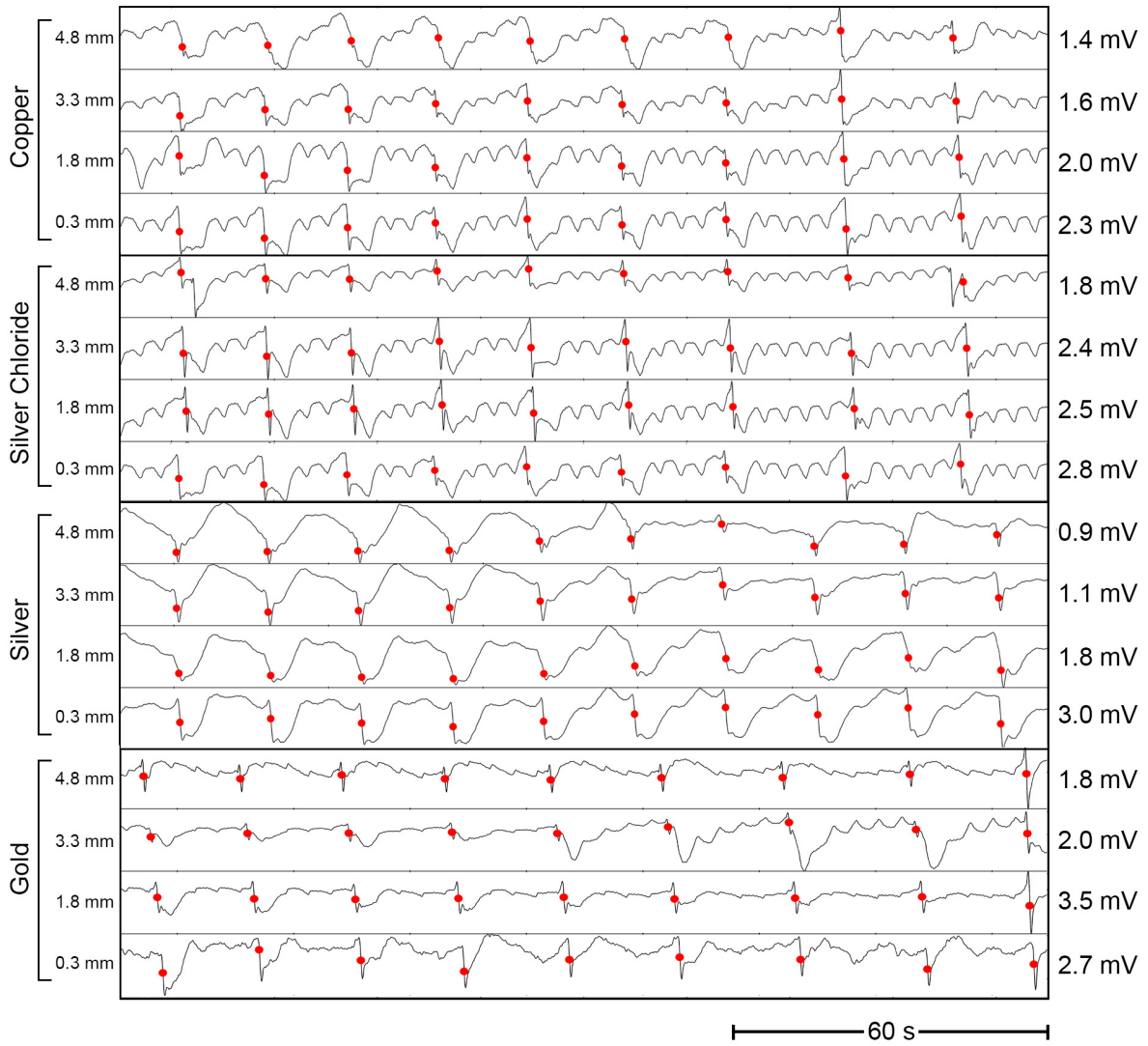

Figure 3: Example electrograms recorded using electrode arrays of copper, silver-chloride, silver and gold from the four diameters, showing the range of typical slow wave signal morphology as well as the temporal characteristics of slow wave recordings. The amplitude values (on right side) show the size of the display window for each electrogram shown.

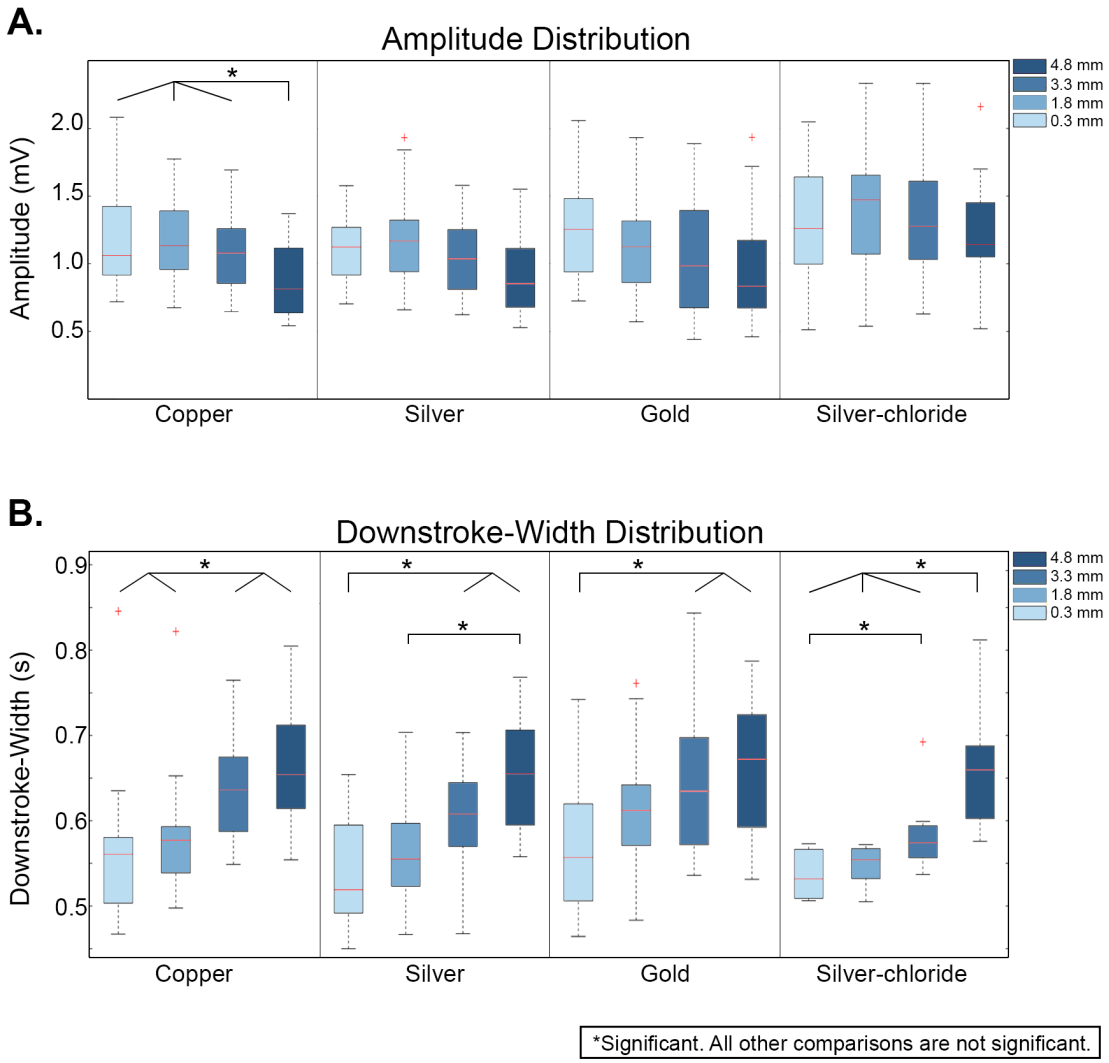

Figure 4: Slow wave amplitudes (A) and downstroke widths (B) from electrodes of different diameter, presented separately for each different electrode material that was trialled in this study. These results demonstrated a general trend of decreasing amplitude with increased electrode diameter, although the trends between the smaller electrode diameters of 0.3 and 1.8 mm were inconsistent (A). The downstroke width consistently increased with increasing electrode diameter across all electrode materials (B). See also Supplementary Table S1.

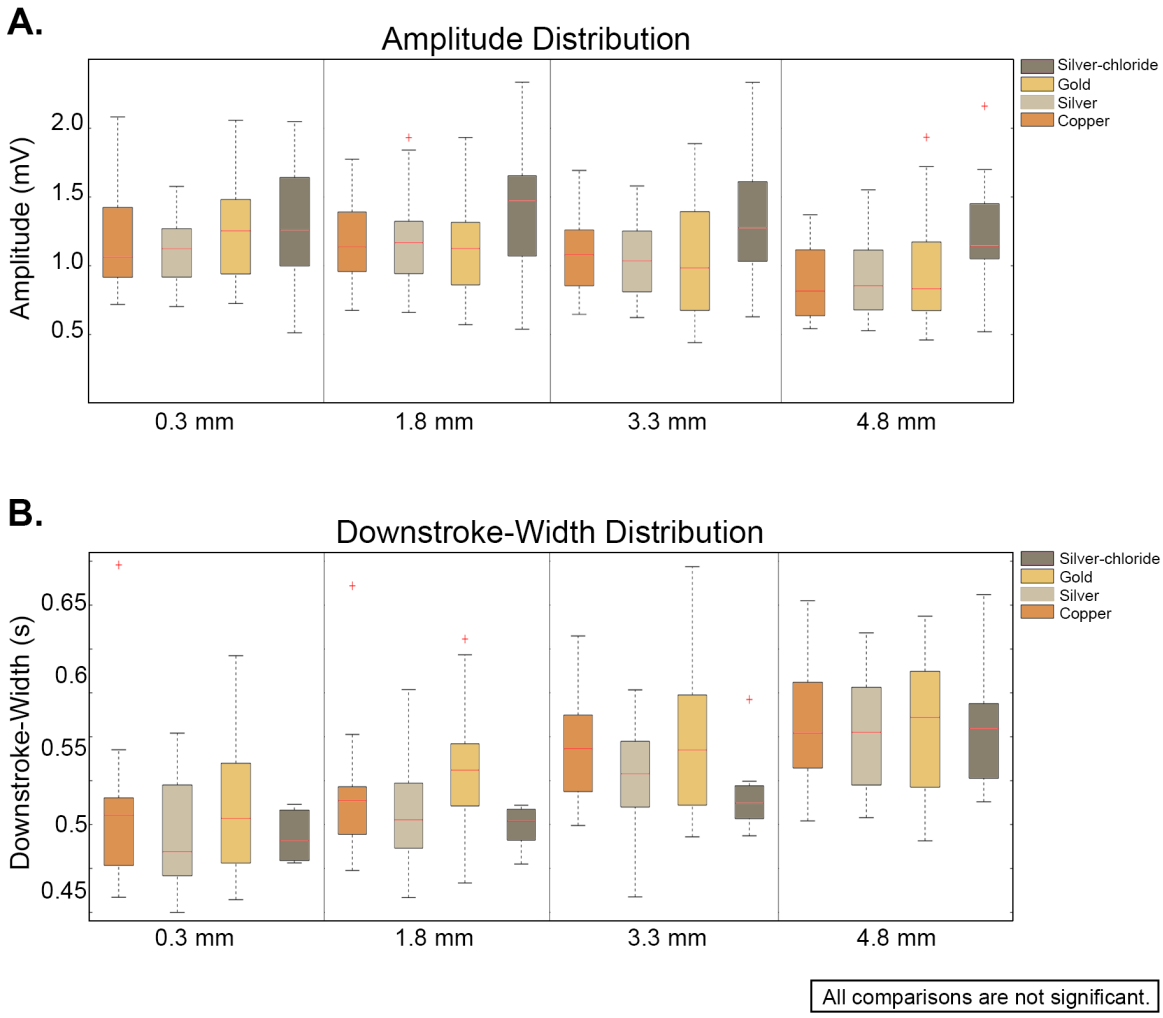

Figure 5: Slow wave amplitudes (A) and downstroke widths (B) from electrodes of different contact materials, presented separately for each different electrode diameter that was trialled in this study. These results demonstrate an increased amplitude obtained from silver-chloride electrodes compared to other materials. There were no consistent trends for downstroke width across the different materials. See also Supplementary Table S1.

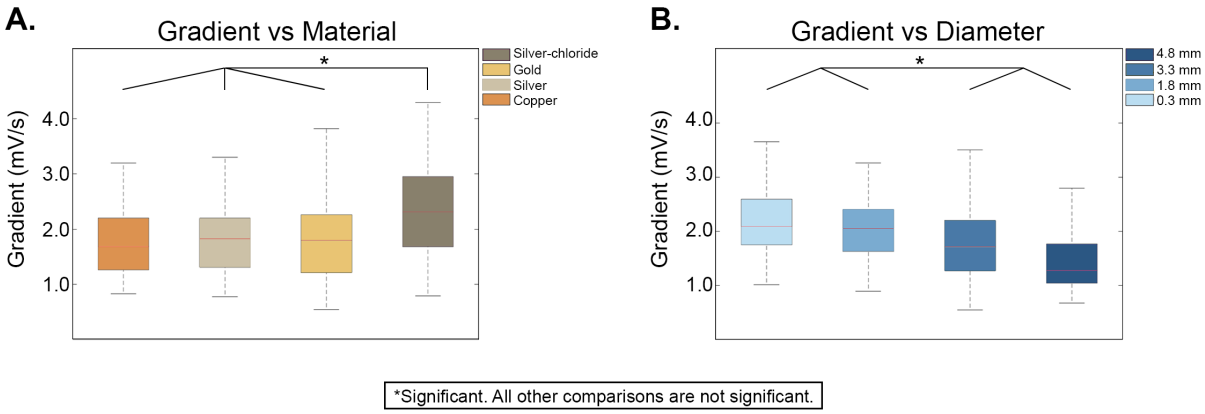

Figure 6: Average slow wave gradients compared across: **A.** the different electrode materials (with all diameters averaged together), and **B.** the different electrode diameters (with all materials averaged together). Silver-chloride electrodes recorded slow wave signals with a statistically significant higher gradient than all other materials, and electrodes of diameter 0.3 and 1.8 mm recorded slow wave signals with a statistically significant higher gradient than the larger diameter electrodes of 3.3 and 4.8 mm. See also Supplementary Table S2.

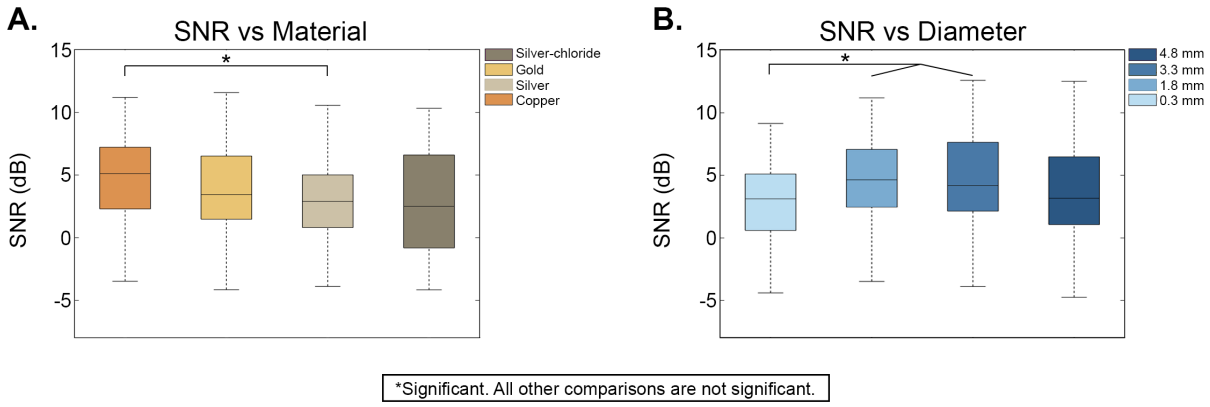

Figure 7: Average SNR of gastric slow wave recordings compared across: **A.** the different electrode materials (with all diameters averaged together), and **B.** the different electrode diameters (with all materials averaged together). Copper electrodes had a statistically significant higher SNR than silver electrodes, but the SNR of signals recorded by all other electrode materials were statistically similar. Electrodes of 1.8 and 3.3 mm diameter recorded signals with a statistically significant higher SNR than electrodes of 0.3 and 4.8 mm diameter. See also Supplementary Table S3.

Supplementary Material:

Supplementary Table S1: Mean slow wave amplitudes and downstroke widths from all electrode materials and diameters tested

Amplitude (mV) (mean ± SEM)					
		Electrode Diameter			
		0.3 mm	**1.8 mm**	**3.3 mm**	**4.8 mm**
Electrode Material	**Copper**	1.18 ± 0.08	1.17 ± 0.07	1.07 ± 0.06	0.89 ± 0.06
	Silver	1.12 ± 0.08	1.20 ± 0.11	1.03 ± 0.08	0.92 ± 0.09
	Gold	1.24 ± 0.08	1.16 ± 0.09	1.02 ± 0.09	0.97 ± 0.09
	Silver-Chloride	1.30 ± 0.17	1.41 ± 0.19	1.35 ± 0.18	1.25 ± 0.17
Downstroke Width (s) (mean ± SEM)					
		Electrode Diameter			
		0.3 mm	**1.8 mm**	**3.3 mm**	**4.8 mm**
Electrode Material	**Copper**	0.56 ± 0.02	0.58 ± 0.02	0.64 ± 0.01	0.66 ± 0.02
	Silver	0.54 ± 0.02	0.57 ± 0.02	0.60 ± 0.02	0.65 ± 0.02
	Gold	0.57 ± 0.02	0.61 ± 0.02	0.64 ± 0.02	0.66 ± 0.02
	Silver-Chloride	0.54 ± 0.01	0.55 ± 0.01	0.58 ± 0.02	0.66 ± 0.03

Supplementary Table S2: Gradient values for all electrode materials and diameters tested.

	Material			
	Copper	**Silver**	**Gold**	**Silver-Chloride**
Gradient (mV/s) (mean ± SEM)	1.80 ± 0.18	1.86 ± 0.18	1.83 ± 0.16	2.32 ± 0.14
	Diameter			
	0.3 mm	**1.8 mm**	**3.3 mm**	**4.8 mm**
Gradient (mV/s) (mean ± SEM)	2.22 ± 0.07	2.19 ± 0.14	1.84 ± 0.16	1.55 ± 0.13

Supplementary Table S3: SNR values for all electrode materials and diameters tested.

	Material			
	Copper	**Silver**	**Gold**	**Silver-Chloride**
SNR (dB) (mean ± SEM)	4.68 ± 0.39	3.14 ± 0.45	3.85 ± 0.41	3.01 ± 1.14
	Diameter			
	0.3 mm	**1.8 mm**	**3.3 mm**	**4.8 mm**
SNR (dB) (mean ± SEM)	2.87 ± 0.44	4.38 ± 0.48	4.65 ± 0.50	3.54 ± 0.52